Laser cladding of manganese oxide doped aluminum oxide granules on titanium alloy for biomedical applications

Xiaoyan Zhang,[a,b†] *Stefan Pfeiffer,*[c,d‡,*] *Pawel Rutkowski,*[e] *Malgorzata Makowska,*[f] *Dariusz Kata,*[e] *Jinlong Yang,*[b] *Thomas Graule,*[c,d*]

[a] Institute for Advanced Materials and Technology, University of Science and Technology Beijing, Beijing 100083, China

[b] State Key Laboratory of New Ceramics and Fine Processing, School of Materials Science and Engineering, Tsinghua University, Beijing 100084, China

[c] Laboratory for High Performance Ceramics, Empa-Swiss Federal Laboratories for Materials Science and Technology, Überlandstrasse 129, 8600 Dübendorf, Switzerland

[d] Institute of Ceramic, Glass and Construction Materials, TU Bergakademie Freiberg, Agricolastraße 17, 09599 Freiberg, Germany

[e] Department of Ceramics and Refractories, Faculty of Materials Science and Ceramics, AGH University of Science and Technology, al. Mickiewicza 30-059 Krakow, Poland

[f] Photon Science Division, Paul Scherrer Institute, 5232 Villigen, PSI, Switzerland

Abstract

Due to the low hardness and poor tribological behavior of titanium alloys, surface coating is a very critical technique in order to increase their commercial exploitation. In this case, Al_2O_3-based coatings are very promising for these alloys to improve their surface properties. To increase the absorption of the laser light in the visible range, MnO_2 is proposed as a dopant for Al_2O_3, in order to achieve dense coatings on Ti6Al4V substrates via cladding with a JK fiber laser. To ensure a homogeneous doping, MnO_2 and Al_2O_3 were dispersed by means of ammonium citrate, and to fully cover the substrate, spray dried MnO_2 doped Al_2O_3 granules were prepared and applied to the substrate. The effects of the solid loading on the properties of these granules were investigated. It is found that with 1.0 wt.% MnO_2 addition, a dense and uniform Al_2O_3 layer, accompanied with an interlayer, was successfully fabricated through laser cladding with low laser power of 20 W. Owing to the better adhesion on the substrate, Al_2O_3 coating on sandblasted substrates feature a higher hardness of 1204.1±66.9 HV0.05 and an elastic modulus of 212.0±11.8 GPa, which is an increase of 165.5 % and 53.3%, respectively, compared to the as-received substrate.

***Keywords*:** Spray drying; MnO_2 doping; Al_2O_3 granules; Ti6Al4V substrate; laser cladding

---

† Xiaoyan Zhang and Stefan Pfeiffer contribute equally to this paper.

* Corresponding author. S. Pfeiffer and Prof. T. Graule

E-mail address: stefan.pfeiffer@empa.ch (S. P.); thomas.graule@empa.ch (T. G.)

1. Introduction

Titanium alloys possess outstanding characteristics such as low density, high strength/weight ratio, high fatigue strength, high fracture toughness, solderability and biocompatibility [1-3]; physical merits that enable these alloys to be broadly applied to aviation, automotive, chemical and biomedical industries. One of the most commonly used titanium alloys is Ti6Al4V, a duplex alloy with 6 wt.% aluminum and 4 wt.% vanadium, which attracts much attention due to its significant role as a biomedical metallic material. It has been implemented in technologies such as artificial bones and joint replacement for repairing tissues; this is due to its good corrosion resistance and elastic modulus, which is closer to the value of bones in comparison to other metallic biomaterials [4]. However, the weaknesses of Ti6Al4V alloy such as low hardness and poor tribological behavior, etc., limit its further applications. Most importantly, the corrosion susceptibility in vivo and vitro environments could lead to the dissolution of vanadium and aluminum ions, further causing implant loosening and finally failure, and even some diseases such as Alzheimer's disease or cancer [5, 6]. Therefore, surface treatments are necessary for Ti6Al4V alloys to enhance their hardness, tribological behavior and corrosion resistance. Coating with Al_2O_3 is recognized as a viable surface treatment approach, owing to its high strength and hardness, excellent wear resistance, low thermal conductivity, high-temperature stability and bio-inert properties [7].

To overcome the shortcomings of various substrates (magnesium alloy, aluminum alloy, Ni-based superalloy, steels, titanium alloy), studies investigating alumina coating have been conducted [8-10], which aim at improving the wear and corrosion properties. Generally, physical vapor deposition (PVD), plasma electrolytic oxidation (PEO), and laser cladding are commonly selected techniques employed to achieve an alumina coating. During the past years, laser cladding processes have attracted extensive attention as a typical coating technology for high-performance surface modification, which fabricate the desired layer through melting the preset powders on the substrate via a high-energy laser beam and then solidification [11]. The laser cladding technique has considerable superiority compared to other coating techniques, and has the major advantage of being able to accurately control the working area, since the spot of the laser can be guided with high spatial resolution over the sample surface. Moreover, as an advanced surface modification technique, the coatings from laser cladding also possess excellent bonding between the coating and matrix [12]. The properties of the laser beam, including spatial and temporal coherence, low divergence, high continuous or pulsed power density and monochromaticity could, also affect the performance of the final coating [6, 13]. Furthermore, functional grade coatings could be realized by laser cladding techniques [14].

Laser cladding of pure alumina ceramic coatings on the surface of an alloy is rarely used in practice, as cracks are easily formed during processing. Thermal stresses generated from high temperatures and cooling rates by high laser power, result in a thermal expansion mismatch between the coating and matrix, leading to the weak bonding state of the coatings [5, 7]. Generally, resolutions, including the

combination with metallic elements [5] or design about a transition layer, are proposed to circumvent these problems, e. g., Gao et al. designed Al-Si alloy to perform as transition layer in the preparation of Al_2O_3 coatings on magnesium alloy [15]. Besides, a variety of additives including Ni, SiO_2, CaO, Cr_2O_3, TiC and TiO_2 were introduced to improve the fracture toughness or wear resistance of the Al_2O_3 coating [10, 16-20]. Wu et al. demonstrated that Al_2O_3-13 wt.% TiO_2 coatings, directly cladded on Ti-6Al-4V substrates by coaxial laser cladding, display a high hardness, good wear resistance and stable performance at elevated temperature [21].

As the most significant manganese oxides, MnO_2 is unstable during the increase of sintering temperature, where the transition to Mn_2O_3 above 530°C and to Mn_3O_4 above 1000°C is observed in air atmosphere [22]. MnO_2, which serves in this work as a dopant to improve the absorption of alumina to the infrared laser light, is also a common additive for Al_2O_3 ceramics, in order to improve the sintering performance by replacing aluminum cations with manganese cations with different valency states in the lattice, which results in fast diffusion lowering the energy necessary for sintering. A density of almost 99% was reached when sintering temperatures rise up to 1650°C and increased hardness and flexural strength were observed [23]. MnO_2 addition could increase the sintering rate as well, and the diffusion mechanism changes from a grain boundary process to a bulk diffusion process [24]. Moreover, the addition of MnO_2 could obviously decrease the sintering temperature of Al_2O_3 ceramics from 1700°C to 1250°C and increase their densification [25-27], further leading to a less time-consuming preparation of high-performance ceramics. Ucar et al. [28] utilized SiO_2 and MnO_2 as additives to enhance the friction and wear behavior of Al_2O_3 ceramics. Wu et al. proposed a novel and feasible route to improve the mechanical properties of SLS-formed porous mullite ceramics using MnO_2 and phenolic resin coated double-shell powders [29].

The behavior of MnO_2 as dopant of alumina was already tested either in vitro or in vivo conditions. Pabbruwe et al. [30] observed a significantly enhancement of osteogenesis within MnO_2-doped alumina tubes (0.5 and 5 mol% manganese) implemented into female rats for 16 weeks. Afterwards, Manganese was not detected by electron microprobe analysis in tissues adjacent to the implanted tubes in vivo. This could be due to immobilization of manganese in alumina, since manganese cations can replace the aluminum cations in the lattice [23, 31]. Furthermore, manganese is a known dopant for hydroxyapatite based bioceramics to accelerate bone formation [32] and to improve the fracture toughness [33]. However, it is proven that an overexposure by high manganese concentrations can be neurotoxic [34].

In this work, MnO_2 was chosen to improve the absorption of the applied laser light, since alumina has only 3% absorption at a wavelength of 1064 nm. To our best knowledge, studies regarding the addition of MnO_2 to Al_2O_3 coatings via a laser cladding process have never been reported. In this study, to further improve the performance of the Al_2O_3 coating, we firstly synthesized homogeneously MnO_2 doped Al_2O_3 granules by a spray drying process, and then analyzed the effects of MnO_2 dopant addition on the properties of the produced Al_2O_3 layer on the Ti6Al4V alloy via the laser cladding technique. By means

of MnO_2 addition, the necessary laser power for the formation of an alumina layer could be lowered drastically.

2. Experimental procedure

2.1 Materials

The raw materials consisted of the high temperature stable α-alumina powder AA03 and nano-scale manganese oxide powder US3319 (98% purity), which were purchased from Sumitomo Chemical Co. LTD, Tokyo, Japan and US Research Nanomaterials, Houston, USA respectively. Alumina is a well-known bioinert ceramic. The dopant manganese oxide combines the advantages of a high absorbance of visible light and the replacement aluminum cations in the lattice with manganese cations [23, 31]. Thus only a small amount of manganese oxide is required to consolidate the alumina layer with low laser power. By immobilization of this small amount of manganese in the alumina lattice, a health risk in biomedical applications can be excluded. To achieve a homogeneous dispersion of alumina and manganese oxide particles, ammonium citrate dibasic p.a. 98% was selected and supplied by Sigma Aldrich Corp., St. Louis, USA. PEG 35000 from Sigma Aldrich Corp., St. Louis, USA was used as binder. Titanium alloy (Ti6Al4V standard alloy, Grade 5) substrates of 1 mm thickness were supplied by BIBUS Metals AG, Fehraltdorf, Switzerland. Throughout the study, deionized Nanopure water was used as the dispersion solvent. Ammonia aqueous solution from Carl Roth GmbH + Co. KG, Karlsruhe, Germany was employed to adjust the pH value of suspension.

2.2 Preparation of MnO_2 doped Al_2O_3 granules

As illustrated in Fig. 1, the spray drying process in combination with laser cladding process was performed to deposit a uniform coating of manganese doped alumina on titanium alloy. It is crucial to guarantee a uniform laser photon absorption and thus a resulting homogenous heat distribution within the whole powder layer. These requirements were fulfilled by a two-step process to produce a dense and homogeneously doped powder bed. Firstly, the dispersion process was optimized in order to prepare a homogeneously doped Al_2O_3 slurry, and secondly the spray drying parameters were refined to produce spherical granules to increase flowability and therefore ensure an even distribution of granules on the substrate. These steps supplied comparable and favorable conditions for the subsequent laser cladding process, where the granules were grit wise consolidated by a fiber laser.

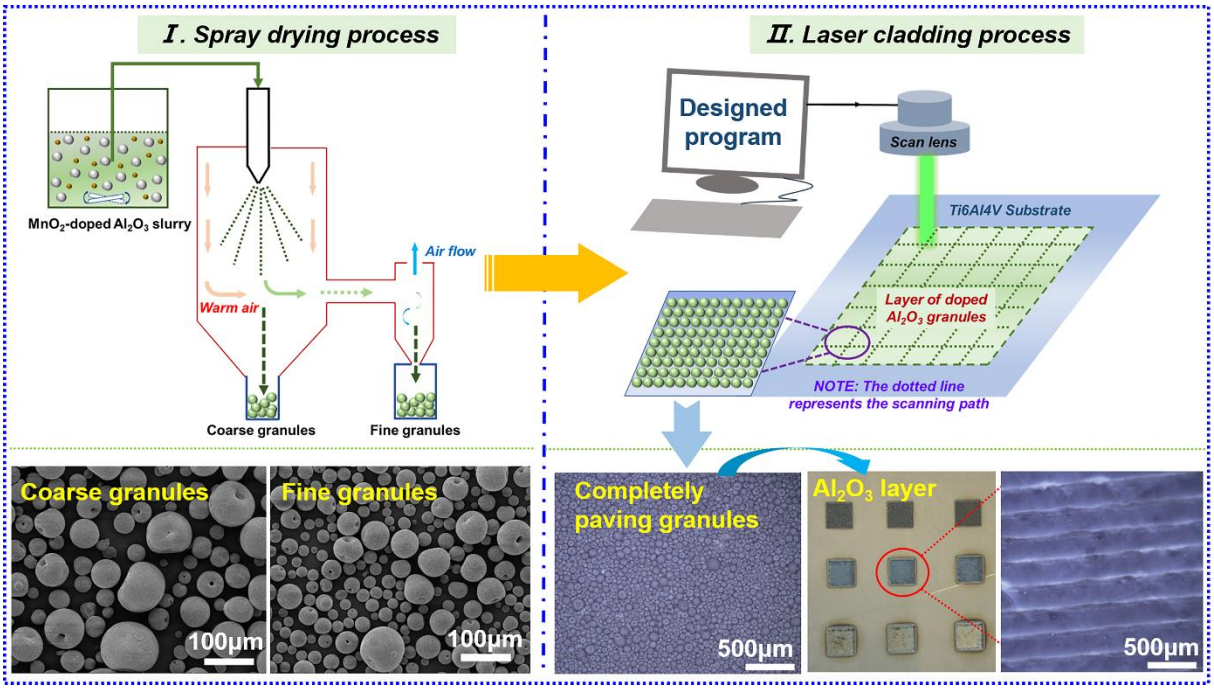

Fig. 1 Schematic illustration of the synthesis process for MnO_2-doped Al_2O_3 layer on the Ti6Al4V alloy

Herein, a conventional lab spray drying technique (Mini spray dryer B-290, Büchi Labortechnik AG, Flawil, Switzerland) was applied to prepare the Al_2O_3 granules with homogeneously doped MnO_2.The fabrication of uniformly dispersed MnO_2 doped Al_2O_3 slurry is a critical factor in the formation process, since for high absorption of the incident light the nanoparticles should be well distributed within the Al_2O_3 matrix [35]. Firstly, MnO_2 nanoparticles were dispersed into deionized water to obtain 10 vol.% MnO_2 suspension. Based on the mass of MnO_2 particles, 1.5 wt.% dispersant was added into the above suspension, as well as zirconia beads (Tosoh Corporation, Tokyo, Japan) with a mean diameter of 0.4 mm (the mass ratio of MnO_2 to zirconia beads was 1:2). Then, a proper amount of diluted ammonia solution was added precisely, dropwise, into the MnO_2 suspension to adjust the pH value to around 8.0, followed by vibration milling for 20 minutes with a vibrational frequency of 30 s^{-1}. Subsequently, the MnO_2 suspension was transferred to ball milling for 24 h. Meanwhile, Al_2O_3 slurries were prepared by mixing Al_2O_3 powder, 0.4 wt.% dispersant and 2.0 wt.% binder (the concentration is calculated based on the mass of Al_2O_3 powder), and their pH values were all controlled to 8.0. Also, Al_2O_3 slurries underwent ball milling for 24 h together with 1.0 mm zirconia beads. Afterwards, the Al_2O_3 slurry and MnO_2 suspension were mixed together and subjected to ball milling for another 4 h. Finally, the mixed slurries were delivered to the ultrasonic nozzle by a peristaltic pump and spray dried at a temperature of 140°C. Further optimized process parameters included an outlet temperature of 90°C, an air flow rate of 25 m^3/h, an ultrasonic nozzle power of around 10 W and a slurry feed rate of circa 2 ml/min. A Dehumidifier B-296 (Büchi Labortechnik AG, Switzerland) was used to control the humidity conditions. Fine granules were separated by a cyclone collector, as shown in Fig. 1. The above steps supplied sufficient and favorable conditions of the granular material for the subsequent laser cladding process.

2.3 Preparation of Al_2O_3 coatings on the Ti6Al4V alloy

In order to enhance the adsorption of the Al_2O_3 granules on the substrate, and to remove surface impurities, abrasion of the Ti6Al4V alloy surface was carried out via sandblasting with SiO_2 grit sand. Afterwards the surfaces were cleaned with acetone before laser cladding. For comparison, untreated Ti6Al4V alloy was also used for the laser cladding process. Prior to laser cladding, Al_2O_3 granules were adhered to the substrate by dispensing in ethanol to obtain suspension with a constant concentration of 25 wt.% and using a burette to guarantee a complete coverage of the surface, which produced a layer thickness of approximately 100 μm. Subsequently, a JK Fibre Lasers type JK200FL (GSI Group Laser Division, Rugby, UK) equipped with a hurrySCAN 30 scanning system (SCANLAB GmbH, Munich, Germany) with low power in the range of 20-60 W, a scanning speed of 3 mm/s and a wavelength of 1080 nm was used to deposit the coating according to a grid pattern with an interval of 0.25 mm and a laser spot size of 40 μm. The working area was fixed at 6 mm × 6 mm. The entire preparation process was illustrated in Fig. 1.

2.4 Characterization

The Zeta potential of MnO_2 dispersed in Nanopure water was tested through a Zeta Potential Analyzer (CD-7020, Colloidal Dynamics Co., Ltd., Ponte Vedra Beach, FL, USA). Zeta potential measurements were performed to evaluate a saturation amount of citrate on the powder surface and to adjust the surface charge by creating a negatively charged surface [36]. Absolute densities were measured by helium pycnometry (AccuPyc II 1340, Micromeritics, Norcross/GA, USA) and N_2 adsorption isotherms were measured at 77 K followed by BET analysis (Brunauer–Emmett–Teller) (SA 3100, Beckman Coulter, Krefeld, Germany) to determine the specific surface area (SSA). The BET average particle size was calculated from the density and specific surface area according to the Sauter mean diameter [37]. Morphologies of particles and coatings were observed by Scanning Electron Microscopy (VEGA3 Tescan, Tescan instruments, Brno, Czech Republic). Before analyzing the cross-sections, the samples were cold embedded in a resin (CaldoFix-2, Struers GmbH, Birmensdorf, Switzerland), ground, polished (with a 1 μm diamond suspension) (Struers Tegramin 30, Struers GmbH, Birmensdorf, Switzerland) and afterwards sputtered with gold-palladium. Particle size distributions of the obtained granules were measured by laser scattering (LS 13320, Beckman Coulter GmbH, Krefeld, Germany). The apparent density of the granules was tested with a setup (PTL Dr. Grabehorst GmbH, Stadtsteinach, Germany) in accordance to DIN EN ISO 23145-2. A jolting volumeter (JEL STAVII, J. Engelsmann AG, Ludwigshafen, Germany) was used to measure the tapped density of granules by tapping 1000 times according to EN ISO 787-11. The absolute densities of granules were characterized by a helium pycnometer (AccuPyc II 1340, Micromeritics, Norcross/GA, USA). The flowability was calculated and rated based on the Hausner ratio, where the tapped density is divided by the apparent density. The residual moisture content of the granules was measured

with the moisture analyzer HR83 (Mettler Toledo GmbH, Greifensee, Switzerland) by applying 140°C for 1 h.

The phase composition of the coatings was characterized by X-ray powder diffraction (XRD) using BRUKER AXS D8 ADVANCE Diffractometer in Bragg-Brentano geometry equipped with Cu-Kα X-ray source. Scanning was conducted in 2θ range of 5°-120° with a step 0.02° and 1s exposure time per step. Analysis of the measured diffraction patterns was performed using TOPAS Bruker AXS software [38]. The chemical composition of the layer was measured using an Orbis PC Micro-XRF Analyzer [39]. Line profiles were obtained by scanning samples with a focused X-ray beam with a 30 μm spot size. The Al_2O_3 coating hardness was tested by a nanoindenter (Fischerscope HM2000, Helmut Fischer GmbH, Sindelfingen, Germany) under a maximum indentation load of 500 mN. The measured diagonal lengths depend on the depth of penetration in relation to the hardness of the material. The diagonal lengths of the remaining indented impression were automatically evaluated by the device. The surface roughness was measured with the fluorescence Stereomicroscope Olympus SZX 16 (Olympus K.K., Tokyo, Japan).

3. Results and discussion

In order to achieve homogeneous MnO_2 doping of the Al_2O_3 granules and to ensure uniform laser photon absorption, a well-dispersed MnO_2 suspension should be initially prepared. Figure 2(a) presents the morphology of MnO_2 particles with an average particle size less than 200 nm, which agglomerate together to form a bigger sphere with a diameter around 10 μm. The measured specific surface area was 22.72 m^2/g, and measured density was 4.28 g/cm^3. With regard to these values, the calculated BET average particle size was 52.5 nm. According to Fig. 2(b), it is shown that the MnO_2 suspension, when free of dispersant, possess an isoelectric point (IEP) of 7.14, and its zeta potential value changes from 43.96 mV to -20.62 mV when the pH value increases from 3 to 9. The initial pH of the dispersion was 4.8, where the zeta potential was 39.9 mV. To modify the surface charge of the particles, ammonium citrate dibasic (ACD) was employed as a specifically adsorbing dispersant and the effect of its added amount on the surface charge properties was investigated. ACD was chosen to disperse both materials with the same dispersant, since it also offers a high affinity to alumina [36]. Results of the zeta potential measurements illustrate that with addition of ACD, the MnO_2 particles become negatively charged and their IEP decreases correspondingly up to 2.78. Besides, more ACD addition promotes the improvement of MnO_2 dispersibility, but no obvious changes were found as ACD increases to 2.0 wt.%, which explains why we choose 1.5 wt.% ACD as the final addition amount. On the other side, various milling approaches have significant influence on the dispersion of MnO_2 nanoparticles, thus vibration milling, roll milling as well as ultrasonic treatment were studied. As shown in Fig. 2(c), a combination of vibration milling and roll milling facilitated an improved dispersion of the MnO_2 particles, since their values of d_{10}, d_{50} and d_{90} (85.5 nm, 131.5 nm, 189.2 nm, respectively) are the lowest, compared to the previously

described techniques performed in isolation. A narrow particle size distribution in the range of 70-200 nm was achieved in Fig. 2(d), which is consistent with the morphology of MnO_2 particles in Fig. 2(a) and a d_{50} of 131.5 nm. This was around 2.5 times bigger than the calculated BET average particle size of 52.5 nm and showed a good dispersion of the particles in water. However, this also indicates that some agglomerates are still present. The evaluation of the zeta potential with and without the addition of ACD to alumina AA03 has already been performed in previous work [35]. The saturation amount to cover the surface was 0.4 wt.% of the dispersant. The zeta potential at pH=8 was -95.5 mV. By roll milling for 24 h, a d_{50} of 303.9 nm with laser scattering was reached with this optimized amount, which was in accordance to the BET average particle size of 269.2 nm calculated from a density of 4.02 g/cm^3 and an SSA of 5.5 m^2/g.

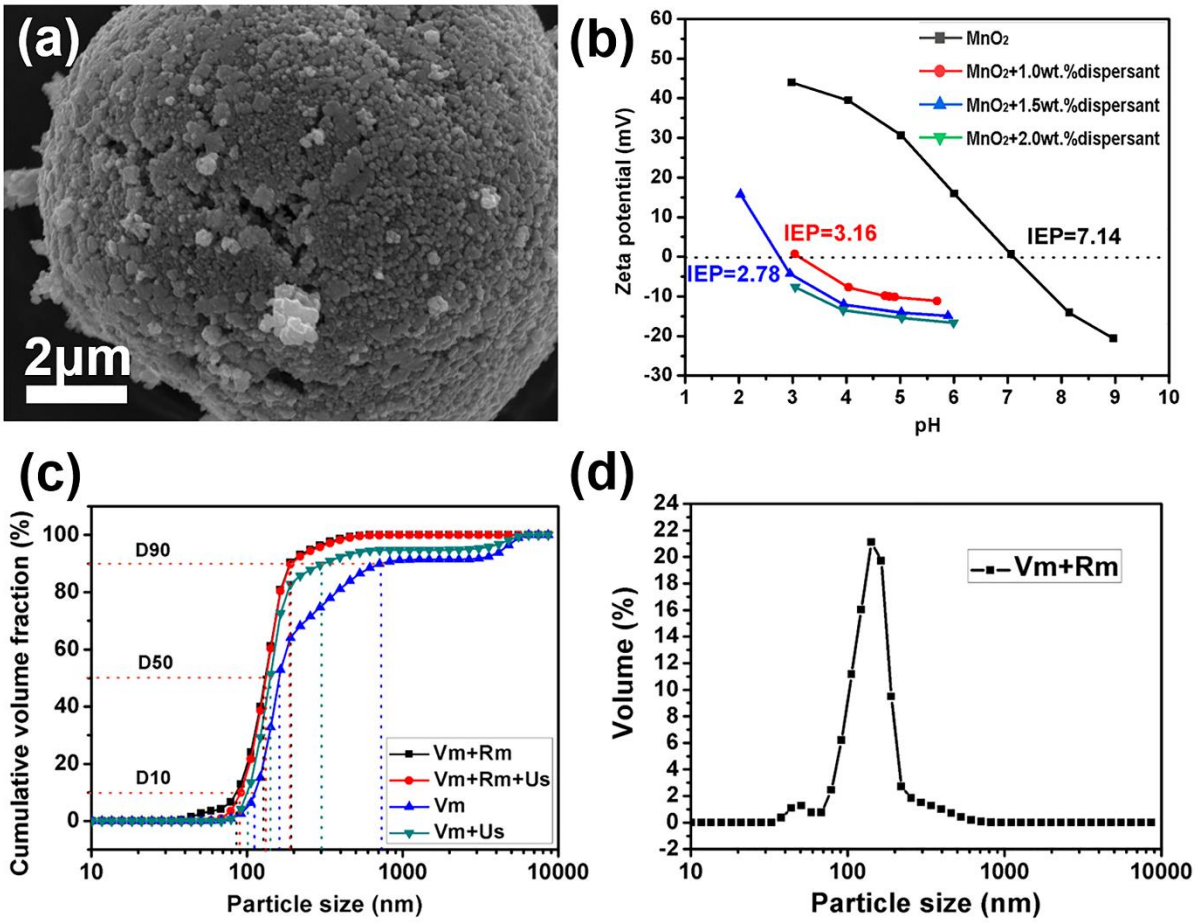

Fig. 2 (a) SEM images of unmodified MnO_2 particles; (b) Zeta potential of MnO_2 suspension as a function of dispersant (ammonium citrate dibasic) amount; (c, d) Volume-based differential DLS particle size distribution of MnO_2 dependent on different milling approaches. ("Vm" represents Vibration milling for 20 min with the frequency of 30 s^{-1}; "Rm" represents Roll milling for 24 h; "Us" represents Ultrasonic treatment for 1.5 min.)

Based on the well-dispersed MnO_2 suspension, doped Al_2O_3 slurries with various solid loadings (35 vol.%, 40 vol.%, 45 vol.%) have been prepared and then spray dried to synthesis spherical granules. Their morphologies are clearly shown in Fig. 3(a-d), demonstrating that the granules are composed of spheres with a distribution of different sizes, with some containing pit-like structures, which resemble macropores. It is found that with an increase of solids loading, the sphericity increases, and the particle size distribution becomes narrower, as is indicated by Fig. 3(e). The maximum size was less than 150 μm. Moreover, the obtained coarse granules (screened with a 180 μm sieve) display larger particle sizes, with d_{50} equal to 75.4 μm, while the correlated fine granules show smaller particle sizes, with a d_{50} equal to 43.7 μm. In view of the spray drying process, schematically shown in Fig. 1, the coarse granules are separated from fine ones mainly due to the particle's weight overcoming the laterally separating driving force of the air flow. Subsequently the fine granules (Fig 3(a-c)) were separated from the air flow with the aid of a cyclone.

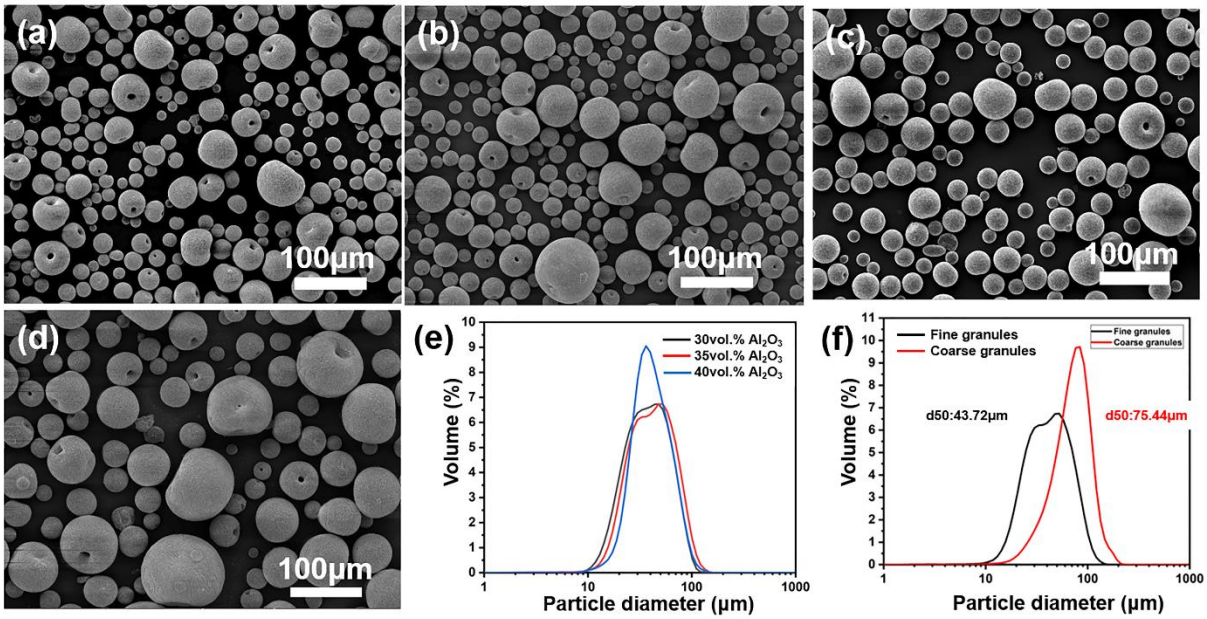

Fig. 3 SEM images of MnO_2-doped Al_2O_3 granules from the spray-drying process: (a) fine granules with 30 vol.% Al_2O_3 slurry, (b) fine granules with 35 vol.% Al_2O_3 slurry, (c) fine granules with 40 vol.% Al_2O_3 slurry, (d) coarse granules with 35 vol.% Al_2O_3 slurry; Particle diameter distribution of granules prepared from various (e) solid loadings and (f) collection approaches. (All granules were prepared with 1.0 wt.% MnO_2)

Table 1 shows the physical properties of various granules, including the densities, moisture content and Hausner ratio. Since the coarse granules experienced less drying time and because of their larger size, their moisture content was the highest of 1.36 wt.%. The Hausner ratio of the granules prepared from slurries with 35 vol.% and 40 vol.% solids loading was slightly lower than that prepared from slurries with 30 vol.% solids loading. The lower Hausner ratio indicates a better flowability, which

should ensure a better coverage and subsequently a denser powder bed on the substrate before the laser cladding process. Besides, the apparent density and tapped density of granules from 35 vol.% slurry were the highest, indicating that this solid loading of the bimodal distribution in water gave the most suitable slurry conditions for spray drying. Finer particles could fill the interstices of the coarse particles and the voids of the bigger granules could be filled by the smaller ones. Moreover, according to the morphology and particle size distribution results presented in Fig. 4, the MnO_2 amount only has a small effect on the granules' properties. It is notable to point out that when the added MnO_2 amount varies from 0 to 1.0 wt.%, the true density and Hausner ratio of obtained granules remain nearly constant.

Table 1. Properties of MnO_2-doped Al_2O_3 granules prepared with different slurries

Samples			Moisture content wt%	Apparent density g/cm^3	Tapped density g/cm^3	True density g/cm^3	Hausner ratio
Solid loading vol.%	Collection way	MnO_2 amount wt.%					
30	Fine	1.0	0.55	1.18±0.01	1.39±0.01	3.86	1.18±0.02
35	Fine	0	0.38	1.19±0.01	1.36±0.02	3.83	1.14±0.01
35	Fine	0.1	0.97	1.21±0.01	1.38±0.01	3.82	1.14±0.01
35	Fine	0.5	1.04	1.20±0.01	1.37±0.05	3.82	1.14±0.04
35	Fine	1.0	0.60	1.23±0.01	1.40±0.02	3.82	1.14±0.01
35	Coarse	1.0	1.36	1.17±0.02	1.35±0.02	3.85	1.15±0.03
40	Fine	1.0	0.50	1.14±0.01	1.30±0.02	3.84	1.14±0.03

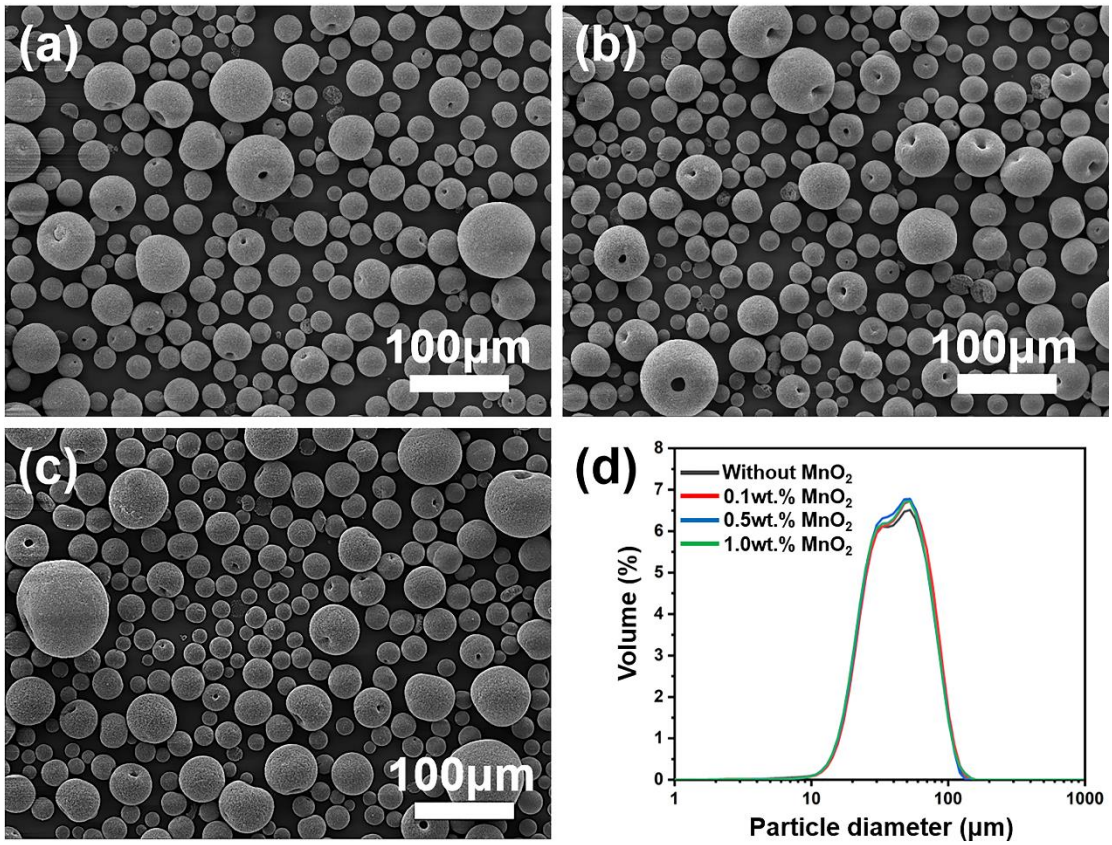

Fig.4 SEM images of granules prepared from Al_2O_3 slurries with increasing amounts of MnO_2: (a) 0wt.%, (b) 0.1wt.%, (c) 0.5wt.%, (d) particle diameter distribution of granules prepared from varied MnO_2 amounts (all samples prepared with 35vol.% Al_2O_3 slurry).

Figure 5(a) shows layers prepared via laser cladding on the alloy substrates as function of different laser powers and granules with different MnO_2 amounts. MnO_2 doping is very crucial for the layer consolidation under low laser power of 20 W. No layer could be achieved when laser cladding was carried out for pure Al_2O_3 granules without a doping of MnO_2, while a black coating was exhibited by samples with 1.0 wt.% MnO_2 addition, irrespective of sandblasted or as-received Ti-alloy substrates. The interaction between the granules without doping was weak since alumina has low absorbance in the visible range and no firmly bonded connection between the ceramic and the metallic substrate could be achieved. Notably, because of a low laser power of 20 W, the thin titanium alloy substrate, with a thickness of 1 mm, suffered nearly no deformation or obvious color change on their back after the processing of granules doped with 1 wt% MnO_2, which results from element diffusion or oxidation. With high laser powers (40 W and 60 W), deformations and color changes were observed. To confirm the composition of the layer, XRF line scans for elements distribution measurements were performed and the results are shown in Fig. 5(b-i). Surface line scans were conducted on the samples prepared from laser powers of 20 W, 40 W and 60 W, and periodic curves perpendicular to the laser path were distinctly found in their optical morphology. The difference among the three samples lies in the concentration distribution of elements including Al, Ti, V, Mn. Results show that a higher concentration of Al tends to be located between two laser line scans on the samples. Besides, distribution of the element Mn shows a similar pattern, while Ti and V display the opposite trend with that of Al. However, the peaks of the manganese concentration are more pronounced than that of aluminum. Considering the composition of granules and substrate, the conclusion could be drawn that the alloy has been well-coated with Al_2O_3. This could be also verified by the elements' distribution from the XRF line scan close to the surface, as shown in Fig. 5(d, e), since a considerable amount of Al was present there. The peaks of Al and Mn in the transition area between two laser line scans could result from temperature differences, since the maximum temperatures during processing were in the center of the processed laser line.

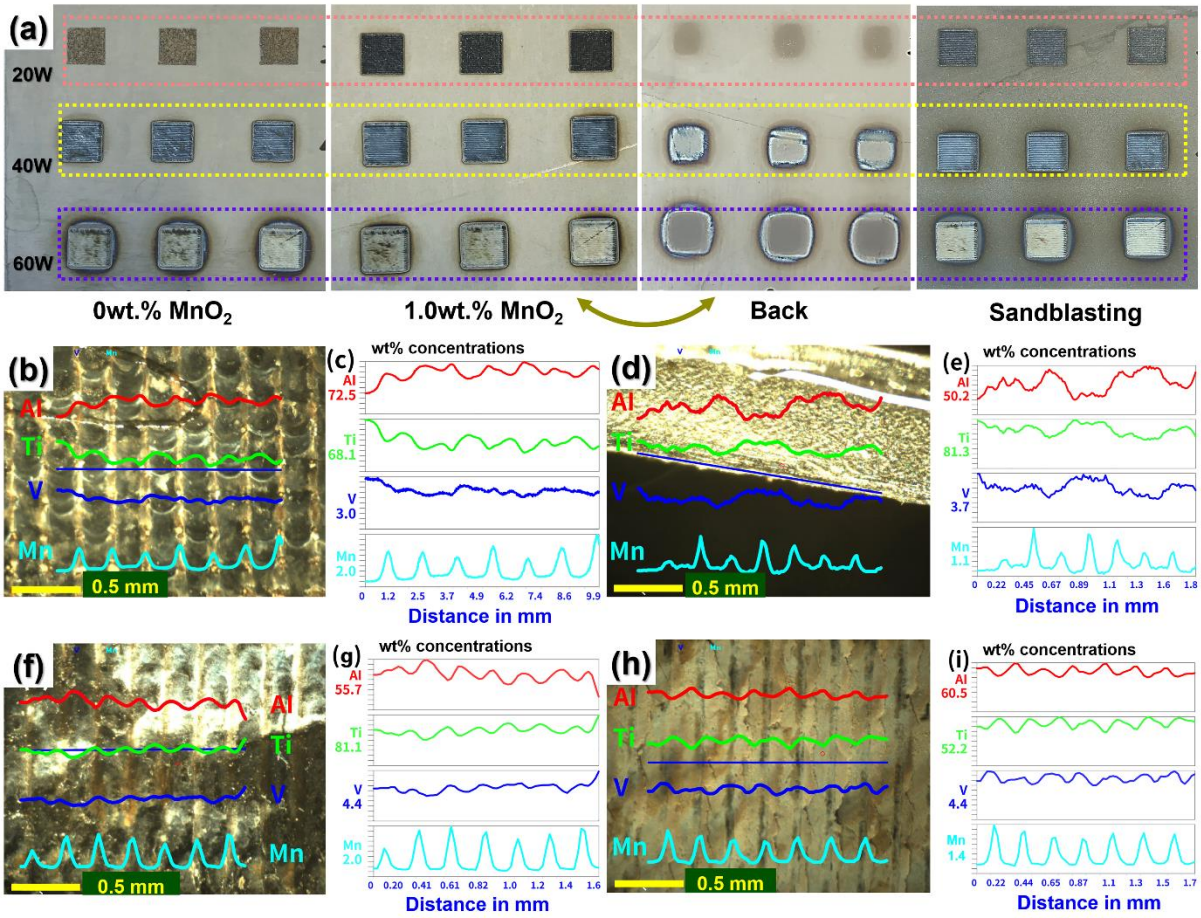

Fig. 5 (a) Photographs of layers prepared by the laser cladding technique; Optical microscopy of the layer surface with the scan path in blue (b) and the cross section (d), the corresponding surface XRF line scan curves (c) and (e); (prepared with laser power of 20 W); Optical microscopy of the layer surface (f) prepared with laser power of 40 W, (h) prepared with laser power of 60 W and the corresponding surface XRF line scan curves (g, i). (All samples are prepared with 1.0 wt.% MnO_2 addition to alumina)

The XRD patterns revealing the crystalline phase composition of the samples produced from varied laser power treatments are shown in Fig. 6. It is found that with 1.0 wt.% MnO_2 addition, no matter how much of the laser power (20 W, 40 W or 60 W) was applied, the major observed phases were α-Al_2O_3, but also of α phase (hcp) of Ti64 and a small quantity of Al_2TiO_5, demonstrating an Al_2O_3 layer has been successfully achieved after laser cladding. A considerable amount of Ti64 α-phase is attributed to the substrate. During laser cladding, Al_2O_3 granules will crystallize firstly on the interface between substrate and paved granules, and α-Al_2O_3 phase forms [7]. In view of laser treatment in the air, TiO_2 could be generated easily with the aid of high temperature and oxygen. Subsequently, α-Al_2O_3 phase will react with TiO_2 to form Al_2TiO_5 [40, 41]. As a high-temperature phase, Al_2TiO_5 phase was still retained, which could be attributed to the fast cooling rate during laser cladding, resulting in a non-equilibrium solidification process [42].

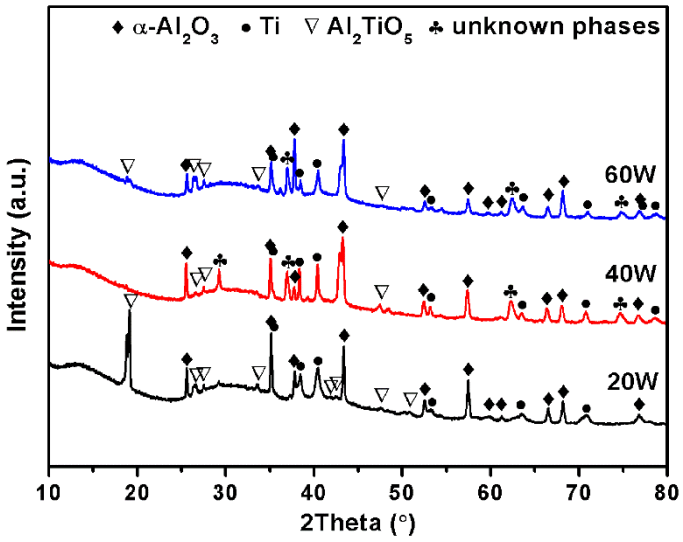

Fig. 6 XRD patterns of samples prepared at various laser powers with 1.0 wt.% MnO_2 addition

The morphology of the layer cross section of samples prepared with laser power of 20 W is clearly shown in Fig. 7(a) and (b). The latter one was polished with a 1 μm diamond suspension. We can conclude that a dense layer around 48.9 μm has been synthesized under 20 W laser power, which is well adhered on the substrate. In addition, EDX patterns of four points from different positions away from the surface have been characterized (Fig. 7(c)). The amount of Al and O decreases when the distance from the layer surface increases, while the amount of Ti and V show the opposite trend in general. Fig. 7(d) clearly shows the gradually varied elements distribution along the marked line. An interlayer composed of moderate amounts of Al and Ti, and with a thickness of around 17 μm, has been detected. With reference to a thickness of ca. 100 μm of the layer before processing and considering the thickness of the interlayer, the shrinkage of the Al_2O_3 layer (real thickness of 31.9 μm) was 68.1%, which is in accordance with the granules tapped density of 36.6% of the theoretical material density. This indicates a dense layer, since the excess of Al_2O_3 (4.7%) could be involved in the interlayer reaction during processing. Due to the reaction between Al_2O_3 and the oxidized substrate, an interlayer forms, which provides a strong adhesion of the coating to the substrate. It is most likely, that the dopant amount of 1.0 wt% was high enough to melt the alumina during laser cladding with a laser power of only 20 W. Consequently, the titanium alloy close to the interface also partly melted as indicated by the formation of the large transition areas in Fig 7(b) and 8(b).

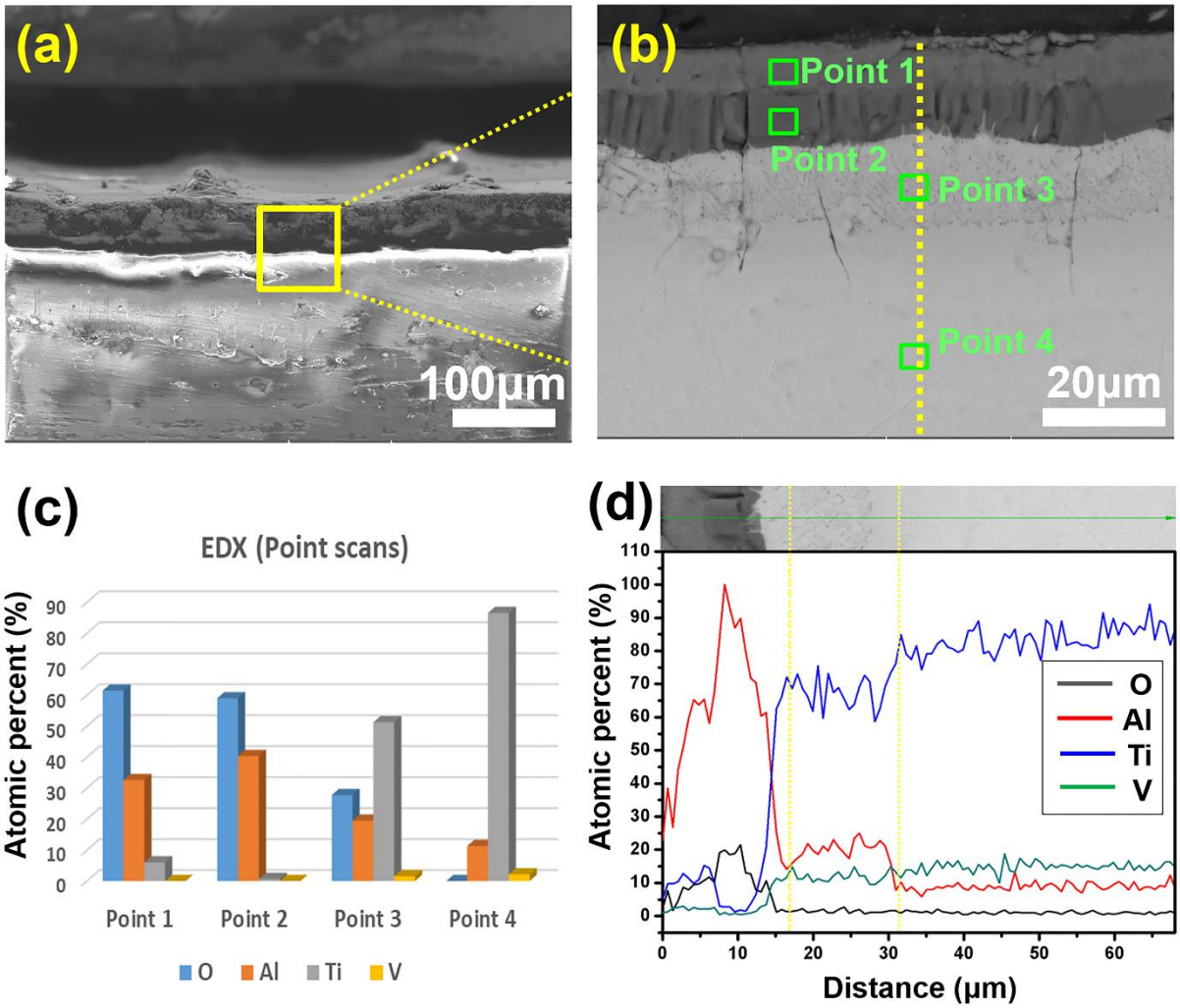

Fig. 7 (a) SEM image of layer cross section prepared via 20 W laser and its BSE image (b), (c) EDX patterns of the marked points in (b) and (d) elements line scan curves vertical to the surface.

Along with the increase of the laser power to 40 W, a thicker Al_2O_3 layer around 117 μm could be deposited on the top of substrate, as shown in Fig. 8(a). Meanwhile, there are several apparent cracks, which are penetrated with melted substrate material in the prepared layer. This confirms the assumption that with a laser power of 40 W the temperature at the interface exceed the melting temperature of the Ti6Al4V alloy, and the metallic phase is in a molten state in the regions near the interface. This phenomenon was not seen with a laser power of only 20 W. Although a higher laser power facilitated a thicker Al_2O_3 layer deposited by laser cladding, the accompanying higher temperature gradient would undoubtedly pose a thermal barrier during the process and magnify the harmful effect of thermal stress caused by the mismatch between layer and substrate. In combination with the EDX point and line scans (figure 8 (b-d)), it could be verified that an interlayer of approximately 40 μm exists in the sample prepared from laser power of 40 W. Therefore, the calculated shrinkage of the Al_2O_3 layer was 23%, thus this layer possess porosity of around 40.4%, which could weaken the mechanical properties of the coating. However, the fewer microcracks in the microstructure of the 40 W processed layers (Fig. 8(b))

compared to the microstructure of the layers processed with 20 W (fig. 7(b)) can be explained by this porosity. Due to the emerging porosity, the solidified material is able to expand and contract without forming thermal stresses. In the case of the dense layers processed with 20 W, the limited space for contraction during cooling causes the cracks due to non-relaxed thermal stresses.

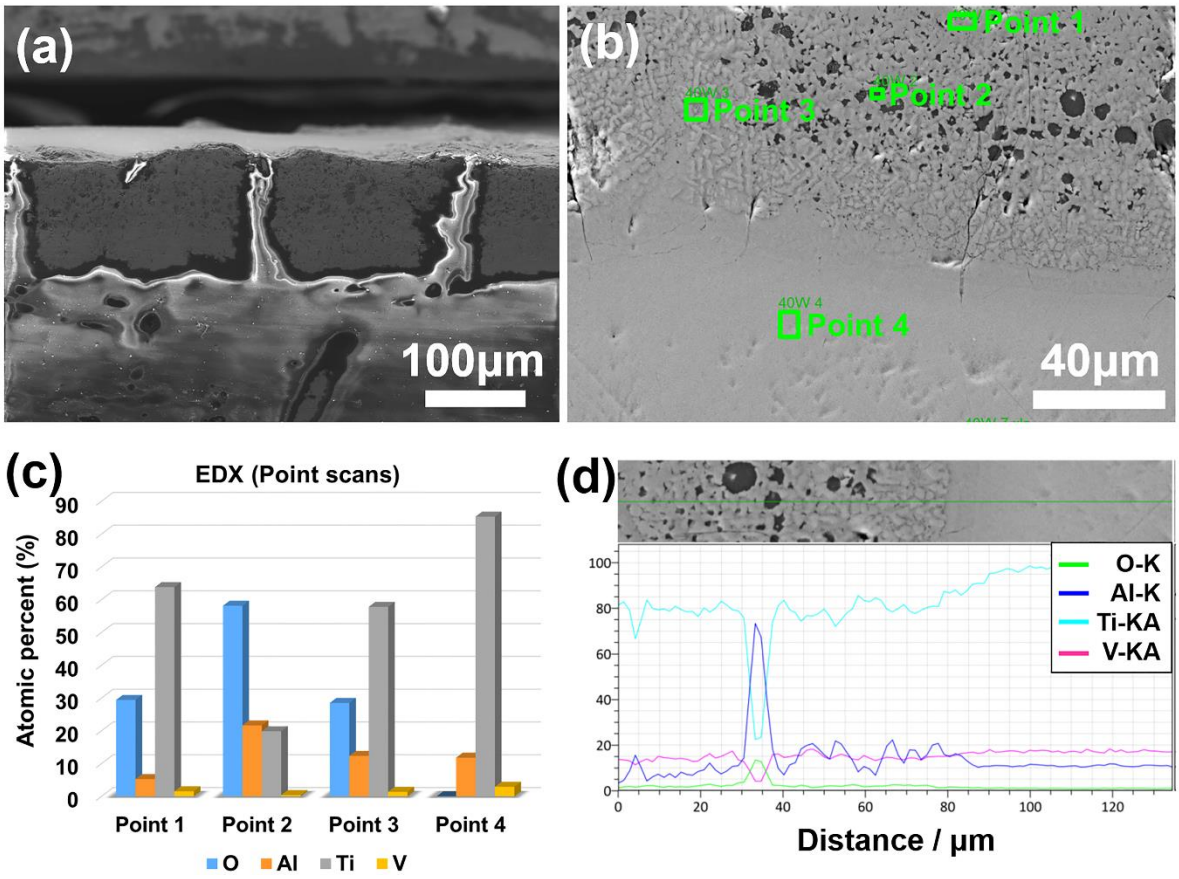

Fig. 8 (a) SEM image of layer cross section prepared via 40 W laser and its BSE image (b), (c) EDX patterns of the marked points in (b) and (d) elements line scan curves vertical to the surface.

Fig. 9(a) demonstrates the microstructure and element compositions of samples prepared using a laser power of 60 W. The elemental composition in Point 1 was 59.11 at.% O, 37.39 at.% Al, 3.25 at.% Ti and 0.25 at.% V. The atomic percent ratio of O to Al is very close to that of Al_2O_3, which is consistent with the result shown in Fig. 6. However, the relative intensity of the layer's diffraction peaks (α-Al_2O_3 phase), compared with that of Ti, increases as the laser power increases. Besides, the concentration of oxygen in the four points marked in Fig. 9(a) decreases gradually from 59.11 at.% to 8.65 at.% as the distance from the top increases. This proves, as well as in the case of the layer processed with lower laser powers, that a severe oxidation of the Ti alloy was avoided during laser cladding, which was most probably achieved by a shielding of the ceramic layer. However, for the samples prepared via 60 W laser power, an interlayer with a higher thickness around 235 µm was formed since the laser could

penetrate more deeply and cause more reaction between the Al_2O_3 with the Ti-alloy substrate. The EDX mapping (Fig. 9(c)) for the cross section in Fig. 9(b) clearly shows that only a thinner coating of Al_2O_3 has been synthesized successfully. The size of the apparent cracks is distinctly increased, compared to the melt-infiltrated cracks in the layers processed with 40 W, which could be due to the higher thermal gradient during processing and the thicker interlayer.

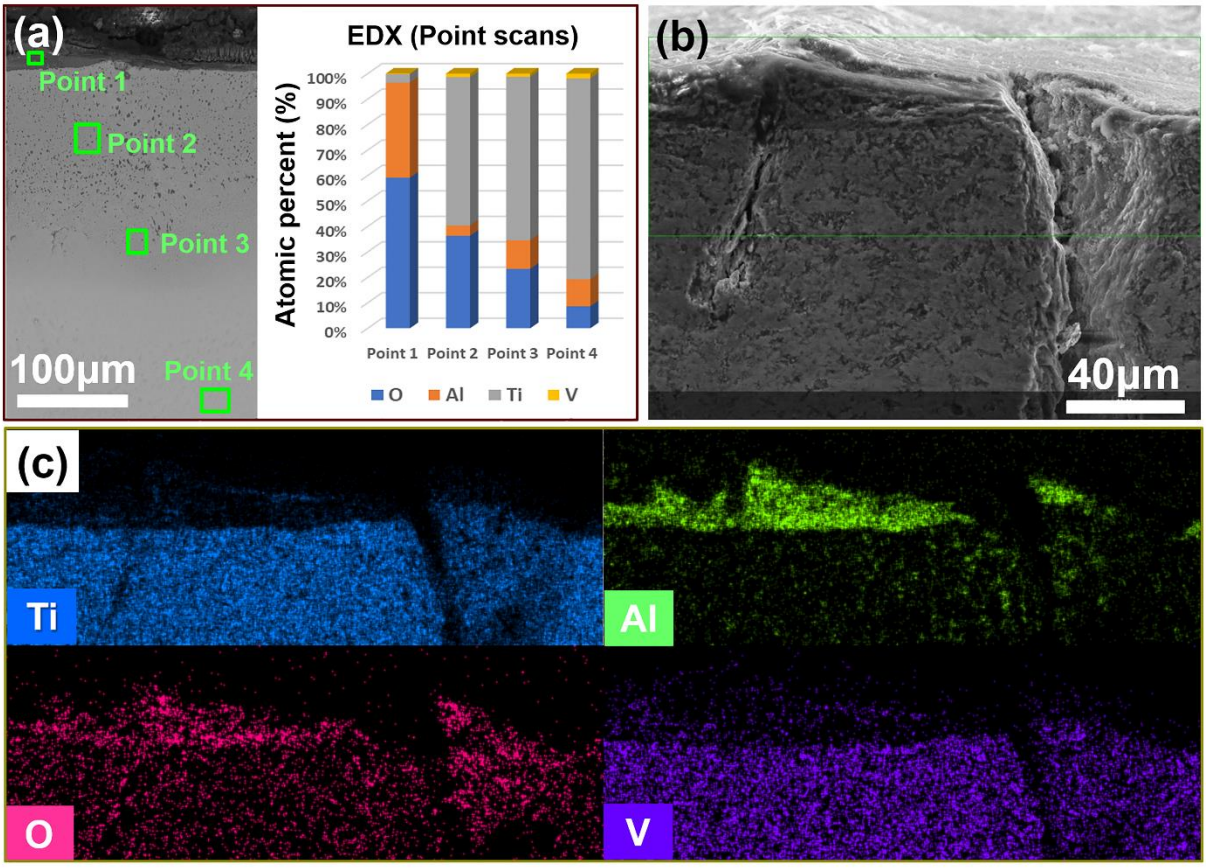

Fig.9 (a) EDX patterns of layer's cross section after polishing prepared via 60 W laser and (b) SEM image with chemical composition showing in (c).

As indicated in Fig. 10(a-d), the surface roughness of the Al_2O_3 coating on the sandblasting substrate was effectively improved from 9.65 µm for that on the as-received substrate to 6.37 µm. It could be assumed that, after sandblasting, spherical granules, especially fine ones, could fill the depression, leading to the perfect combination (increased contact area) with the substrate, which further increases the uniformity, smoothness of the coating after laser treatment. Typical load-displacement curves of the marked position of the coatings on both substrates, are shown in Fig. 10(e). The measurements have been performed on the marked positions in Fig. 10(a) and (c) and include a load-on, holding and load-off segments. At full load, the coating on the as-received substrates exhibits a higher indentation depth. Notably, the obtained Al_2O_3 coating significantly improves the mechanical properties of the Ti6Al4V substrate, for both the as-received or sandblasted samples. Their hardness increases by almost three

times compared to the pure substrate (453.6±135.1 HV0.05 for as received Ti6Al4V substrate and 409.5±194.7 HV0.05 for sandblasted Ti6Al4V substrate), and their elastic moduli also increase greatly. In addition, compared with the Al_2O_3 coating on the as-received substrate, the Al_2O_3 coating on the sandblasted substrate possess higher hardness of 1204.1±66.9 HV0.05 and elastic modulus of 212.0±11.8 GPa. The difference between the elastic moduli is only 8 GPa and within the measurement standard deviation, whereas the hardness differs more significantly by more than 130 HV0.05. However, due to the microcracks formed from interlayer thermal expansion mismatch, the hardness and elastic moduli of the Al_2O_3 coating is lower than the Al_2O_3 ceramics, which have been prepared with the same granules via uniaxial dry pressing method (99.95% density) and sintered at 1600°C for 2 hours. The hardness of these bulk ceramics was 1821.5±200.1 HV0.05 and its elastic moduli was 370.4±12.8 GPa, which are comparable with the literature values (up to 2100 HV0.05 in [43] and 2450 HV0.05 and a Young's modulus of 350 GPa in [44]). In accordance to the porous and cracked morphology observed in the microscopy images presented in Fig. 8, the Al_2O_3 coating prepared from a laser power of 40 W possess an extremely low hardness of 215.2±49.2 HV0.05 and elastic moduli of 107.1±19.0 GPa. This could be mainly due to the porosity most probably generated from a high cooling rate. This result indicates that for the laser cladding process of alumina on Ti-alloy substrates only low laser powers should be used and that manganese oxide serves as effective dopant to decrease the required laser power for consolidation.

Comparable values for HV0.05 were found in different studies for ceramic and ceramic composite layers deposited by laser cladding. Dhanda et al. adopted a preplaced powder mixture method to prepare a multi-component coating (TiC, TiB_2, $NiTi_2$, B_4C, SiC phases are included) on a Ti6Al4V surface, and effectively improved the surface hardness from 364 HV0.05 to 780 HV0.05 with the assistance of a Ytterbium Fibre Laser processed with 1.8 kW [45]. Kumar Sahoo et al. produced a TiC reinforced steel composite layer on a AISI 304 steel substrate with a hardness of 1200 HV0.05 through laser scanning over the preplaced TiC powder by means of a pulse Nd:YAG laser with an average power of 160~168 W [46]. In the presented work, the measured hardness of the specimens produced on the sandblasted substrate (1204.1±66.9 HV0.05) are comparable to these two references. However, different material systems with different expected values for the hardness were used. The biggest difference was distinctly in terms of the used laser power, where only a small fraction was applied in this work. A low energy consumption was realized by employing a small addition of MnO_2, without an obvious effect on the phase composition, and most probably a beneficial effect on diminishing crack formation was observed. Thus, this approach offers new ideas for a successful surface modification of alloys by depositing ceramic coatings via laser cladding.

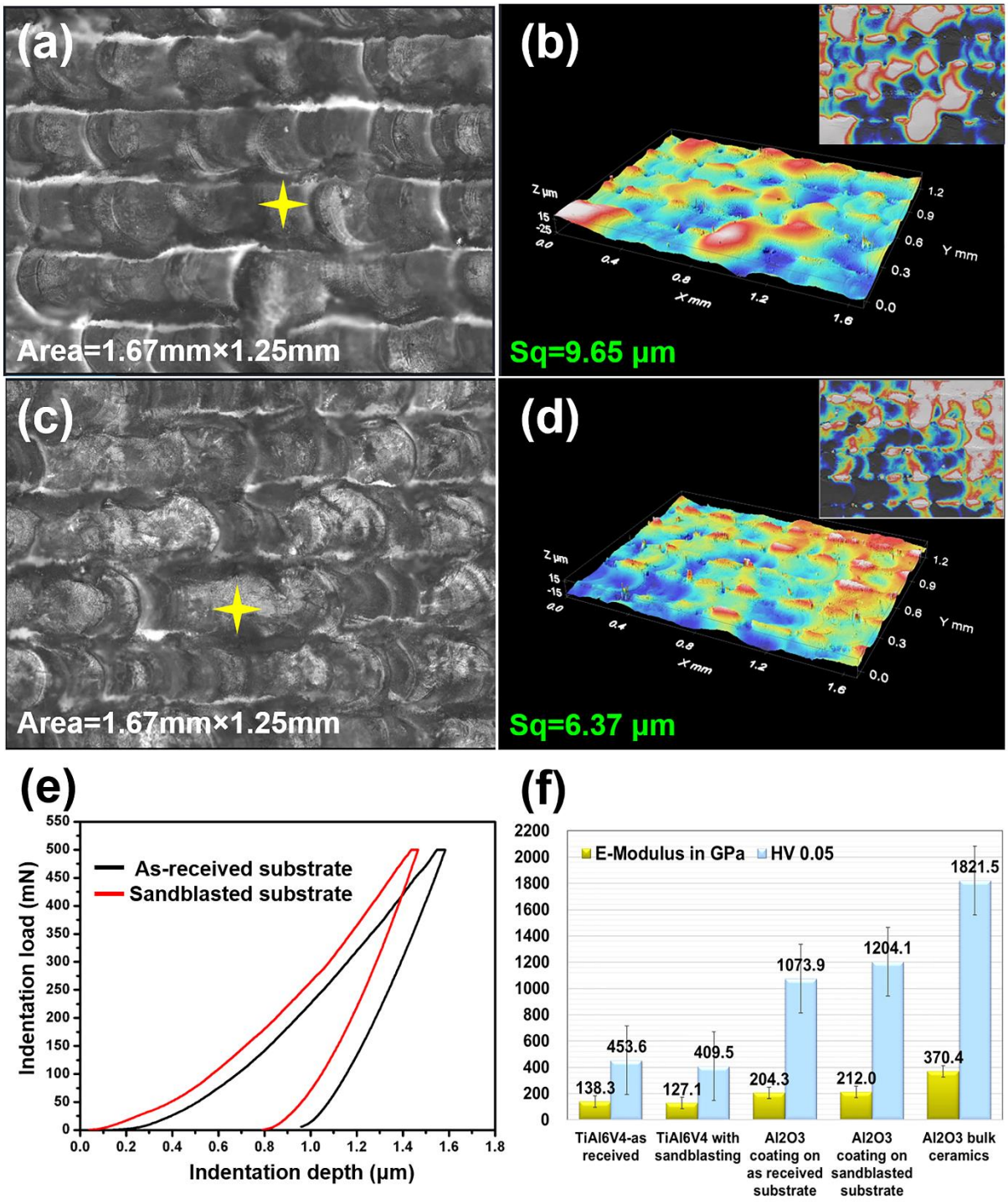

Fig. 10 Three-dimensional stereomicroscope images of coating surfaces prepared under 20 W with the as-received substrate (a, b) as well as the sandblasting substrate (c, d); (e) Nanoindentation load-displacement curves obtained from samples with different substrates; (f) Comparison of hardness and Young's modulus of samples (tested at the marked position in (a) and (c), both were prepared with laser power of 20 W using 1.0 wt.% MnO_2 doped Al_2O_3 granules)

In the case of the titanium alloy, wear is a result of the accumulation of plastic deformation. Theoretical and experimental studies proved that wear resistance has a positive correlation with hardness, which

reflect their ability to resist plastic deformation [47]. This correlation, as well the correlation between increasing hardness with improved corrosion resistance performance, are found for pure Ti6Al4V, as well as for metal matrix composite coatings with embedded ceramic particles and ceramic coatings on titanium alloy substrates [48-50]. For heat-treated Ti6Al4V, an increase of the hardness required superior properties of the polycrystalline diamond milling tools [48]. A Ni/Al_2O_3 composite coating showed improved corrosion resistance and less wear loss compared to the Ti6Al4V substrate due to the higher surface hardness [49]. Cui et al. [50] demonstrated that a high chemical stability and a high ratio of hardness to Young's modulus, which is a measurement that reflects a material's resistance to plastic deformation, provided good tribocorrosion performance of the TiN coating on titanium alloy. Therefore, in this work the laser cladded Al_2O_3 coating on Ti6Al4V alloy with excellent hardness is also promising for applications in biomedical materials research, in order to protect the substrate from wear and corrosion once in an in-vivo environment.

4. Conclusions

Laser cladding of an Al_2O_3 coating on a Ti6Al4V substrate using a low laser power of 20 W has proved to be successful with the aid of a nano-MnO_2 dopant. The MnO_2 addition increased the absorption of the laser light and enabled the formation of alumina layers with significant lower laser energies. Spray-drying of MnO_2 doped Al_2O_3 granules was performed to assure homogeneously doped MnO_2 within the Al_2O_3 matrix, and to achieve full paving of the granules on the substrate. Processing of the powder bed for laser cladding was only possible, when an excellent dispersion of the nanoscale MnO_2 particles in water delivered a high absorption of the IR laser light by the spray dried granules. After laser cladding, a dense and uniform layer of Al_2O_3 with the thickness of 48.9 µm was formed using a laser power of 20 W. To form this layer, a MnO_2 addition of 1.0 wt.% was used. XRD and EDX measurements show a low concentration of Ti in this layer, as well as a small interlayer consisting mainly of Al_2TiO_5 was also detected, and was formed during processing. By the use of higher laser power apparent cracks appeared in the coating layer, which could be formed due to an overheating caused by an avalanche effect of the laser light absorption. Due to the better adhesion of the coating on the substrate, Al_2O_3 coatings on sandblasted substrates possess a higher hardness of 1204.1 HV0.05 and an elastic modulus of 212.0 GPa compared to those on as-received substrates. A significant improvement of the hardness and elastic modulus properties of the substrate could be achieved. This approach is promising for surface modification of alloys by high-quality ceramic coating, since low energy consuming lasers for cladding can be applied due to the increase of absorptivity by a small amount of MnO_2 addition.

Disclosure statement

The manuscript was written through contributions of all authors. All authors have given approval to the final version of the manuscript. The authors declare no competing financial interest.

Acknowledgement

This work was supported by the ETH Board for funding the "FUORCLAM" project within the frame of the SFA (Strategic Focus Areas) Advanced Manufacturing. The authors thank Fundamental Research Funds for the Central Universities (Grants No. FRF-GF-19-032B), China Postdoctoral Science Foundation (Grant No. 2019T120086, 2018M630154). Thanks to Dr. Jon Bell for proof reading the English. The authors would like to acknowledge Dr. Dariusz Gawryluk (Solid State Chemistry Group, PSI) for enabling an access to XRD and XRF measurements techniques.

References

[1] Y.K. Qin, D.S. Xiong, J.L. Li, R. Tyagi, Compositions and tribological properties of PEO coatings on Ti6Al4V alloy, Surf. Eng. 33 (2017) 895-902. doi: 10.1179/1743294414Y.0000000412.

[2] L. Ceschini, E. Lanzoni, C. Martini, D. Prandstraller, G. Sambogna, Comparison of dry sliding friction and wear of Ti6Al4V alloy treated by plasma electrolytic oxidation and PVD coating. Wear, 264 (2008) 86-95. doi: 10.1016/j.wear.2007.01.045.

[3] H. Liu, X. Zhang, Y. Jiang, R. Zhou, Microstructure and high temperature oxidation resistance of in-situ synthesized TiN/Ti_3Al intermetallic composite coatings on Ti6Al4V alloy by laser cladding process. J. Alloy. Compd. 670 (2016) 268-274. doi: 10.1016/j.jallcom.2015.10.168.

[4] C.S. Chien, C.W. Liu, T.Y. Kuo, C.C. Wu, T.F. Hong. Bioactivity of fluorapatite/alumina composite coatings deposited on Ti6Al4V substrates by laser cladding, Appl. Phys. A 122 (2016) 303. doi: 10.1007/s00339-016-9788-1.

[5] A. Mthisi, A.P.I. Popoola, Influence of Al_2O_3 addition on the hardness and in vitro corrosion behavior of laser synthesized Ti-Al_2O_3 coatings on Ti-6Al-4V. Int. J. Adv. Manuf. Technol. 100 (2019): 917-927. doi: 10.1007/s00170-018-2785-0.

[6] N.M. Baloyi, A.P.I. Popoola, S.L. Pityana, Laser coating of zirconium and ZrO_2 composites on Ti6Al4V for biomedical applications. S. Afr. J. Ind. Eng. 25 (2014) 62-70. doi: https://doi.org/10.7166/25-1-661.

[7] D. Wang, Z. Tian, S. Wang, L. Shen, Z. Liu, Microstructural characterization of Al_2O_3–13 wt.% TiO_2 ceramic coatings prepared by squash presetting laser cladding on GH4169 superalloy. Surf. Coat. Technol. 254 (2014) 195-201. doi: 10.1016/j.surfcoat.2014.06.011.

[8] Y. Gao, C. Wang, M. Yao, H. Liu, The resistance to wear and corrosion of laser-cladding Al_2O_3 ceramic coating on Mg alloy. Appl. Surf. Sci. 253 (2007) 5306-5311. doi: 10.1016/j.apsusc.2006.12.001.

[9] T.M. Yue, K.J. Huang, H.C. Man, In situ laser cladding of Al_2O_3 bearing coatings on aluminium alloy 7075 for improvement of wear resistance. Surf. Eng. 23 (2007) 142-146. doi: 10.1179/174329407X169449.

[10] Y. Li, J. Yao, Y. Liu, Synthesis and cladding of Al_2O_3 ceramic coatings on steel substrates by a laser controlled thermite reaction. Surf. Coat. Technol. 172 (2003) 57-64. doi: 10.1016/s0257-8972(03)00255-x.

[11] M. Zhong, W. Liu, Laser surface cladding: the state of the art and challenges. Proc. Inst. Mech. Eng. Part C-J. Eng. Mech. Eng. Sci. 224 (2010) 1041-1060. doi: 10.1243/09544062JMES1782.

[12] B. Yao, C. Wang, R. Wang, C. Jiang, Influence of scanning velocity on microstructure and properties of laser clad NiAlBSi high-temperature alloy coatings, Chinese J. Lasers 38 (2011) 35-40. doi: 10.3788/CJL201138.1003001.

[13] X.X. Duan, S.Y. Gao, Q. Dong, Y.F. Zhou, M.Z. Xi, X.P. Xian, B. Wang, Reinforcement mechanism and wear resistance of Al_2O_3/Fe-Cr-Mo steel composite coating produced by laser cladding. Surf. Coat. Technol. 291 (2016) 230-238. doi: 10.1016/j.surfcoat.2016.02.045.

[14] I. Shishkovsky, I. Smurov, Titanium base functional graded coating via 3D laser cladding. Mater. Lett. 73 (2012) 32-35. doi: 10.1016/j.matlet.2011.12.099.

[15] Y. Gao, C. Wang, M. Yao, H. Liu, Microstructure analysis and numerical simulation of laser cladding Al_2O_3 ceramic coating on magnesium alloy, Appl. Laser 26 (2006) 393-397. doi: 10.3969/j.issn.1000-372X.2006.06.009.

[16] Y. Chen, D. Wu, G. Ma, W. Lu, D. Guo, Coaxial laser cladding of Al_2O_3-13% TiO_2 powders on Ti-6Al-4V alloy. Surf. Coat. Technol. 228 (2013) S452-S455. doi: 10.1016/j.surfcoat.2012.05.027.

[17] H. Zhao, X. Z. Hu, M. B. Bush, Grain growth phenomena in the interface region of alpha-alumina bilayer composites, J. Am. Ceram. Soc. 84 (2001) 1865-1872. doi: 10.1111/j.1151-2916.2001.tb00928.x.

[18] B. Pan, X. Song, W. Huang, B. Wang, C. Li, Research progress of laser cladding Al_2O_3 based coatings on surface of Ti6Al4V alloy, Hot Working Tech. 44 (2015) 19-21. doi: 10.14158/j.cnki.1001-3814.2015.16.005.

[19] H. C. Soo, B. P. Sung, S. K. Dae, Corrosion behavior of plasma-sprayed Al_2O_3-Cr_2O_3 coatings in hot lithium molten salt, J. Nucl. Mater. 399 (2010) 212-218. doi: 10.1016/j.jnucmat.2010.01.022.

[20] J. Gao, J. Suo, Preparation of TiC+(/TiC)+ composite coating by plasma spraying, J. Chin. Ceram. Soc. 39 (2011) 1844-1849. doi: 10.14062/j.issn.0454-5648.2011.11.027.

[21] D. Wu, Y. Chen, W. Lu, G. Ma, Y. Guo, D. Guo, Dilution characters of Al_2O_3-13wt%TiO_2 coating by direct laser cladding on titanium alloy, Rare Metal Mater. Eng. 41 (2012) 2105-2108. doi: CNKI:SUN:COSE.0.2012-12-009.

[22] N.N. Greenwood, A. Earnshaw, Chemistry of the Elements, 2nd ed., Butterworths/Heinemann, Oxford, 1997, pp. 1049.

[23] H. Erkalfa, Z. Misirli, M. Demirci, C. Toy, T. Baykara, The densification and microstructural development of Al_2O_3 with manganese oxide addition. J. Eur. Ceram. Soc. 15 (1995) 165-171. doi: 10.1016/0955-2219(95)93062-8.

[24] J.R. Keski, I.B. Cutler, Initial sintering of Mn_xO-Al_2O_3, J. Am. Ceram. Soc. 51(1968) 440-444. doi: 10.1111/j.1151-2916.1968.tb11915.x.

[25] X.W. Huang, S.W. Wang, S.K. Zhao, X.X. Huang, Effect of liquid-forming additives on the sintering and mechanical properties of Al_2O_3/3Y-TZP (30 vol.%) composite. Mater. Res. Bull. 37 (2002) 1709-1719. doi: 10.1016/s0025-5408(02)00850-4.

[26] I.B. Cutler, C. Bradshaw, C.J. Christensen, E.P. Hyatt, Sintering of alumina at temperature of 1400°C and below, J. Am. Ceram. Soc. 40(2006) 134-139. doi: 10.1111/j.1151-2916.1957.tb12589.x.

[27] H. Erkalfa, Z. Misirli, T. Baykara, Densification of alumina at 1250°C with MnO_2 and TiO_2 additives. Ceram. Int. 21 (1995) 345-348. doi: 10.1016/0272-8842(95)96207-6.

[28] V. Ucar, A. Ozel, A. Mimaroglu, I. Calli, M. Gur, Influence of SiO_2 and MnO_2 additives on the dry friction and wear performance of Al_2O_3 ceramic. Mater. Des. 22 (2001) 171-175. doi: 10.1016/s0261-3069(00)00069-8.

[29] A. Chen, J. Chen, J. Wu, L. Cheng, R. Liu, J. Liu, Y. Chen, C. Li, S. Wen, Y. Shi. Porous mullite ceramics with enhanced mechanical properties prepared by SLS using MnO_2 and phenolic resin coated double-shell powders. Ceram. Int. 45 (2019) 21136-21143. doi: https://doi.org/10.1016/j.ceramint.2019.07.090.

[30] M. B. Pabbruwe, O. C. Standard, C. C. Sorrell, C. R. Howlett, Bone formation within alumina tubes: effect of calcium, manganese, and chromium dopants. Biomaterials 25 (2004) 4901-4910. doi: https://doi.org/10.1016/j.biomaterials.2004.01.005.

[31] I.B. Cutler, Nucleation and Nuclei Growth in Sintered Alumina, in: Kinetics of High Temperature Process Part III, Technology Press of M. I. T. and John Wiley & Sons, 1959, pp. 120-127.

[32] J.I. Kang, M. K. Son, H.C. Choe, W. A. Brantley, Bone-like apatite formation on manganese-hydroxyapatite coating formed on Ti-6Al-4V alloy by plasma electrolytic oxidation. Thin Solid Films 620 (2016) 126-131. doi: https://doi.org/10.1016/j.tsf.2016.07.088.

[33] S. Lala, T. N. Maity, M. Singha, K. Biswas, S. K. Pradhan, Effect of doping (Mg, Mn, Zn) on the microstructure and mechanical properties of spark plasma sintered hydroxyapatites synthesized by mechanical alloying. Ceram. Int. 43 (2017) 2389-2397. doi: https://doi.org/10.1016/j.ceramint.2016.11.027.

[34] S. L. O'Neal, W. Zheng, Manganese toxicity upon overexposure: a decade in review. Current Environmental Health Reports 2 (2015) 315-328. doi:10.1007/s40572-015-0056-x.

[35] S. Pfeiffer, K. Florio, M.G. Makowska, D.F. Sanchez, H.V. Swygenhoven, C.G. Aneziris, K. Wegener, T. Graule, Iron oxide doped spray dried aluminum oxide granules for selective laser sintering and melting of ceramic parts. Adv. Eng. Mater. 21 (2019) 1801351. doi:10.1002/adem.201801351.

[36] P.C. Hidber, T.J. Graule, L.J. Gauckler, Citric acid-a dispersant for aqueous alumina suspensions, J. Am. Ceram. Soc. 79 (1996) 1857-1867. doi: 10.1111/j.1151-2916.1996.tb08006.x.

[37] J. Sauter, Die Grössenbestimmung der im Gemischnebel von Verbrennungskraftmaschinen vohrhandenen Brennstoffteilchen:(Mitteilung aus dem Laboratorium für Technische Physik der Technischen Hochschule München), VDI-Verlag, 1926.

[38] DIFFRAC.SUITE TOPAS-XRD Software, X-ray diffraction-XRD Software | Bruker, [Online]. https://www.bruker.com/products/x-ray-diffraction-andelemental-analysis/x-ray-diffraction/xrd-software/topas.html, 2018 (accessed 04 October 2018).

[39] Orbis PC Micro-XRF Analyzer. https://www.edax.com/products/micro-xrf/orbis-pc-analyzer.

[40] Z. Yao, Y. Liu, Y. Xu, Z. Jiang, F. Wang, Effects of cathode pulse at high frequency on structure and composition of Al_2TiO_5 ceramic coatings on Ti alloy by plasma electrolytic oxidation, Mater. Chem. Phys. 126 (2011) 227-231. doi: 10.1016/j.matchemphys.2010.11.035.

[41] S. Wang, Q. Zhao, D. Liu, N. Du, Microstructure and elevated temperature tribological behavior of TiO_2/Al_2O_3 composite ceramic coating formed by microarc oxidation of Ti6Al4V alloy, Surf. Coat. Technol. 272 (2015) 343-349. doi: 10.1016/j.surfcoat.2015.03.044.

[42] Y. Wang, C.G. Li, W. Tian, Y. Yang, Laser surface remelting of plasma sprayed nanostructured Al_2O_3–13wt%TiO_2 coatings on titanium alloy, Appl. Surf. Sci. 255 (2009) 8603-8610. doi: 10.1016/j.apsusc.2009.06.033.

[43] S. Brust, A. Röttger, W. Theisen, New wear-resistant materials for mining applications, Int. Conf. Stone Concr. (2015) 272-280. doi: 10.13154/icscm.3.2015.272-280.

[44] N. Hezil, M. Fellah, Synthesis and structural and mechanical properties of nanobioceramic (α-Al_2O_3), J. Aust. Ceram. Soc. (2019) 1-9. doi: https://doi.org/10.1007/s41779-019-00333-7.

[45] M. Dhanda, B. Haldar, P. Saha, Development and characterization of hard and wear resistant MMC coating on Ti-6Al-4V substrate by laser cladding, Procedia Mater. Sci. 6 (2014) 1226-1232. doi: 10.1016/j.mspro.2014.07.196.

[46] C. Kumar Sahoo, M. Masanta, Effect of pulse laser parameters on TiC reinforced ISI 304 stainless steel composite coating by laser surface engineering process, Optic Laser. Eng. 67 (2015) 35-48. doi: http://dx.doi.org/10.1016/j.optlaseng.2014.10.010.

[47] B. Bhushan, Modern Tribology Handbook (Chemical Ruther, Boca Raton, FL), Vol. 1, p. 273.

[48] W. Cui, F. Niu, Y. Tan, G. Qin, Microstructure and tribocorrosion performance of nanocrystalline TiN graded coating on biomedical titanium alloy, Trans. Nonferrous Met. Soc. China 29 (2019) 1026-1035. doi: 10.1016/S1003-6326(19)65011-9.

[49] S.A. Abbasi, P. Feng, Y. Ma, J. Zhang, D. Yu, Z. Wu, Influence of microstructure and hardness on machinability of heat-treated titanium alloy Ti-6Al-4V in end milling with polycrystalline diamond tools, Int. J. Adv. Manuf. Technol. 86 (2016) 1393-1405. doi: 10.1007/s00170-015-8245-1.

[50] C.K. Lee, Corrosive wear and mechanical properties of Ni/Al_2O_3 micro- and nanoparticulates-reinforced coatings on Ti-6Al-4V alloy, Tribol. Trans. 55 (2012) 640-651. doi: 10.1080/10402004.2012.689611.